AIAA 91-1664

Unsteady Fluid Dynamic Model For Propeller Induced Flow Fields

Steven Yon and Joseph Katz
San Diego State University,
San Diego, CA
and Dale L. Ashby
NASA Ames Research Center,
Moffett Field, CA

AIAA 22nd Fluid Dynamics, Plasma Dynamics & Lasers Conference
June 24-26, 1991 / Honolulu, Hawaii

AIAA-91-1664-CP

UNSTEADY FLUID DYNAMIC MODEL FOR PROPELLER INDUCED FLOW FIELDS

Steven Yon *, and Joseph Katz**
Department of Aerospace Engineering and Engineering Mechanics
San Diego State University, San Diego, California
and
Dale L. Ashby†,
NASA Ames Research Center
Moffett Field, California

Abstract

A potential flow based three-dimensional panel method was modified to treat time dependent flow conditions in which the body's geometry may vary with time. The main objective of this effort was the study of a flow field due to a propeller rotating relative to a nonrotating body which is otherwise moving at a constant forward speed. Calculated surface pressure, thrust and torque coefficient data for a four-bladed marine propeller/body compared favorably with previously published experimental results.

Nomenclature

A_k	panel surface area
B_k, C_k	influence coefficients
$c(z)$	local blade chord
C_p	pressure coefficient, defined by equation 17
C_Q	torque coefficient (torque/$\rho D^5 n^2$)
C_T	thrust coefficient (thrust/$\rho D^4 n^2$)
D	diameter of propeller
$\vec{F}$	fluid dynamic force
J	advance ratio (V_o/n D)
L	body's length
N	number of panels
n	number of propeller revolutions per second
$\vec{n}$	vector normal to panel surface
p	pressure
R	propeller radius
r	radial distance
$\vec{r}$	vector (x,y,z)
S	area element
t	time
V_o	translational velocity of origin
$\vec{V}$	total velocity vector
v_{ref}	reference velocity used in the Bernoulli equation
x, y, z	body coordinates
β_{TIP}	blade pitch angle measured at r/R=1.0
Γ	circulation
γ	circulation per unit length
η	propeller efficiency ($JC_T/2\pi C_Q$)
θ	rotation about the y axis
μ	doublet strength
ρ	fluid density
σ	source strength
Φ	velocity potential
ϕ	rotation about the x axis
ψ	rotation about the z axis
Ω	rotation rate of body-coordinates

Introduction

Computational methods, based on the solution of the potential flow model (often called 'Panel Methods'), are constantly being refined and are capable of solving problems with complex boundaries. For example, the flow field and the resulting aerodynamic loads on a complete airplane configuration submerged in a steady free-stream can be resolved with the methods of Refs. 1-4. The gradual refinements introduced over the years into these methods mainly affect their numerical efficiency, but incremental improvements of the mathematical model which are aimed at expanding the range of applicability of the fluid dynamic model can also be found. These latter improvements can be in the form of wake rollup routines, interaction with boundary layer solutions or even zonal Navier-Stokes solutions (this last technique is geared mainly toward calculation of flow-separation lines). Another upgrade of these methods, as described in Ref. 5, is made possible by introducing an option for the unsteady motion of a solid body. An upgraded version of this approach resulted in the computer program of Ref. 6 which improved efficiency allowing the program to run on small personal computers. The unsteady motion, at this point, was aimed at maneuvering airplanes for which the path of the motion is known (prescribed) and the geometry of the body was fixed (with time). However, many unsteady fluid dynamic problems require that the geometry of the body vary with the motion. For example, wing flaps may move during aircraft maneuvers, and propeller and rotor blades move relative to the nonrotating fuselage. The ubiquitous nature of problems involving relative motion has resulted in a search for the capability to model such flow fields (even with inviscid flow models). Such an improvement is not difficult from the mathematical point of view but may considerably increase the computational effort in a true unsteady mode (where various body components may move relative to each other).

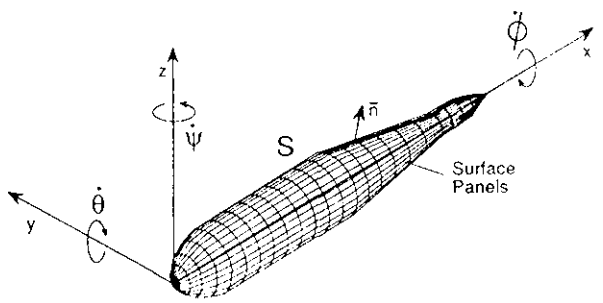

Fig. 1 Body-fixed coordinate system used for the mathematical model.

* Graduate Student, Student Member, AIAA
** Professor, Associate Fellow, AIAA
† Aerospace Engineer, Member, AIAA

Possible methods for modeling propeller induced flow fields are presented in the survey paper by J. E. Kerwin[7]. One widely used approach (which does not result in a considerably increased numerical complexity) is obtained when a steady state panel method is used with only a few local programming modifications. This approach was used sucessfully to modify the Hess code[1] of the Douglas Aircraft Company and has a wide range of applications as presented in Refs. 8-12. Clearly, the steady-state free-stream condition must be exchanged for one that accounts for the propeller rotation. This change effects areas in the computer program such as the pressure calculations and the known part of the boundary condition (often called 'Right Hand Side'). Additionally, a spiral wake shape must be specified, either as an input or by some simplified precalculations.

The approach taken in the current study is to select the time dependent panel method option and consequently the shape of the trailing wake will be determined automatically by a time stepping sequence. For the case of a rotating propeller moving steadily forward this current formulation results in a computationally more efficient model for which no previous knowledge of the wake shape is required. Furthermore, this feature is included for the first time in a widely used panel method[6] which can now be used for the analysis of both steady and unsteady flow fields, without requiring a high level of training for the novice user.

Brief Description of the Fluid Dynamic Model

A detailed description of the mathematical principles of Panel Methods is rather lengthy and can be found in publications such as Refs. 1-2, 4, or Ref. 6 and in text books such as Ref. 13. Therefore, the following description of the model is by no means complete and is aimed only at highlighting the major steps leading to the numerical formulations and the differences between this and the previous[1-4] methods.

The following model is based on the assumption that for high Reynolds number attached flows, viscous effects are confined to thin boundary layers and wakes, and that the lifting properties of wings and propellers can be estimated by solving the potential flow problem. With this assumption in mind, the fluid surrounding the submerged body shown in Fig. 1 is assumed to be inviscid, irrotational, and incompressible over the entire flow field, excluding the body's solid boundaries and its wakes. For this case then, the continuity equation in terms of the velocity potential Φ becomes

$$\nabla^2\Phi = 0 \tag{1}$$

The interesting observation at this point is that Eq. 1 does not include time derivatives. Any time dependency will therefore be introduced through the boundary condition requiring zero normal velocity across the body's solid surface:

$$(\nabla\Phi - \vec{V}_o - \vec{\Omega}\times\vec{r})\cdot\vec{n} = 0 \tag{2}$$

$$(in \quad x,y,z \quad body \quad coordinates)$$

where $\vec{V}_o$ is the translational velocity of the (x,y,z) body system's origin, resolved into the instantaneous x, y, and z directions, $\vec{r} = (x,y,z)$ is the position vector and $\vec{\Omega}$ is the rate of rotation of the body's frame of reference,

$$\vec{\Omega} = (\dot{\phi},\dot{\theta},\dot{\psi}) \tag{3}$$

Since Eq. 1 is elliptic the boundary conditions must be specified on the boundaries enclosing the entire fluid region. Therefore, a second boundary condition is specified at the far field boundaries and requires that the flow disturbance due to the body's motion through the fluid must vanish far from the body

$$lim\nabla\Phi_{|\vec{r}|\to\infty} = 0 \tag{4}$$

For the unsteady flow case the use of the Kelvin condition will supply an additional equation which can be used to determine the streamwise strength of the vorticity shed into the wake. In general, it states that in the potential flow region the angular momentum cannot change, thus the circulation Γ around a fluid curve enclosing a lifting surface and its wake is conserved

$$\frac{d\Gamma}{dt} = 0 \quad (for\ any\ t) \tag{5}$$

The amount of circulation generated by a lifting surface can be fixed by applying the steady state Kutta condition along the trailing edges of lifting surfaces

$$\gamma_{T.E.} = 0 \tag{6}$$

This condition is assumed to be reasonable as long as the flow is attached on the propeller blades. The wake shape and rollup can be determined by requiring that the velocity vector $\vec{V}$ should be parallel to the wake circulation vector γ_W

$$\vec{\gamma}_W \parallel \vec{V} \tag{7}$$

The solution to the problem presented in Eqs. 1, 2, and 4 can be solved using Green's second identity which states that a general solution to Eq. 1 can be constructed by integrating the contribution of the basic solutions of source σ and doublet μ distributions over the body's surface and its wakes:

$$\Phi(x,y,z) = \frac{1}{4\pi}\int_{body+wake}[\mu\vec{n}\cdot\nabla(\frac{1}{r}) - \sigma(\frac{1}{r})]dS \tag{8}$$

This singular element solution automatically fulfills boundary condition 4.

For thick bodies, the condition of zero flow across solid boundaries can be satisfied by using the Dirichlet formulation which states that the inner perturbation potential is assumed to be constant such that

$$\Phi_i = const. \tag{9}$$

By selecting $\Phi_i = 0$ for the perturbation velocity potential (or $\Phi_i = \Phi_\infty$ for the total potential) Eq. 8 becomes[2,4,13]

$$\frac{1}{4\pi}\int_{body+wake}\mu\frac{\partial}{\partial n}(\frac{1}{r})dS - \frac{1}{4\pi}\int_{body}\sigma(\frac{1}{r})dS = 0 \tag{10}$$

This equation still does not uniquely describe a solution since a large number of source and doublet distributions will satisfy a set of such boundary conditions. A frequently followed choice for panel methods (e.g. PMARC[6]) is to set the value of the source distribution equal to the local kinematic velocity (the time dependent equivalent of the free-stream velocity).

$$\sigma = -\vec{n}\cdot(\vec{V}_o + \vec{\Omega}\times\vec{r}) \tag{11}$$

At this point the mathematical problem is unique and can be solved. From the numerical point of view, the body's surface is divided into rectilinear surface panel elements (as shown in Fig. 1) and for each panel Eq. 10 is satisfied at a collocation point placed at the center of the panel (inside the body, at least in principle). By rewriting the Dirichlet boundary condition (Eq. 10) for each of the N collocation points Eq. 10 will have the following form:

$$\sum_{k=1}^{N}\frac{1}{4\pi}\int_{body-panel}\mu\vec{n}\cdot\nabla(\frac{1}{r})dS + \sum_{\ell=1}^{Nw}\frac{1}{4\pi}\int_{wake-panel}\mu\vec{n}\cdot\nabla(\frac{1}{r})dS$$

$$-\sum_{k=1}^{N}\frac{1}{4\pi}\int_{body-panel}\sigma(\frac{1}{r})dS = 0 \tag{12}$$

That is for each collocation point (of each panel shown in Fig. 1) the summation of the influences of all k body panels and ℓ wake panels is needed. The integration is limited now to each individual panel element, and for a unit strength singularity element (σ or μ), it depends on the panel's geometry only. For example, for a constant strength μ element, the influence of panel k at an arbitrary point P can be represented by the influence coefficient C_k

$$\frac{1}{4\pi}\int_{Panel\ area}\frac{\partial}{\partial n}(\frac{1}{r})dS\ |_k \equiv C_k \tag{13}$$

Similarly for a constant strength σ element, the source influence B_k is defined by

$$\frac{-1}{4\pi}\int_{Panel\ area}(\frac{1}{r})dS\ |_k \equiv B_k \tag{14}$$

Therefore, the Dirichlet boundary condition on each collocation point of a thick body (Eq. 10) can be reduced to the following form

$$\sum_{k=1}^{N} C_k\mu_k + \sum_{\ell=1}^{N_W} C_\ell\mu_\ell + \sum_{k=1}^{N} B_k\sigma_k = 0 \tag{15}$$

which must hold at any time t.

The time dependent solution generally proceeds as follows: first, the wake shedding trailing-edge panels are identified (as a programmer input). The constant strength doublet panel (which is used for the wake, too) is equivalent to a closed vortex ring along the panel edges, and therefore, the Kelvin condition (Eq. 5) is satisfied for all time steps. The calculation then begins as an initial value problem and at the first time step one wake row is shed from the propeller trailing edges. The strength of the wake panels is specified in terms of the trailing edge doublet values through Eq. 6. So, at the first moment, the geometry of the body and of the wake is known and Eq. 15 can be specified. For a geometry involving N panels, N unknown doublet values are obtained (by solving the boundary condition specified at the N collocation points). During the next time step, the body's geometry and position are changed according to a prescribed motion path and the wake shape is modified. To achieve the wake rollup at each time step, the induced velocity $(u,v,w)_\ell$ at each wake panel corner point ℓ is calculated (usually in the undisturbed flow frame of reference) and then the vortex elements are moved by

$$(\Delta x, \Delta y, \Delta z)_\ell = (u,v,w)_\ell \Delta t \tag{16}$$

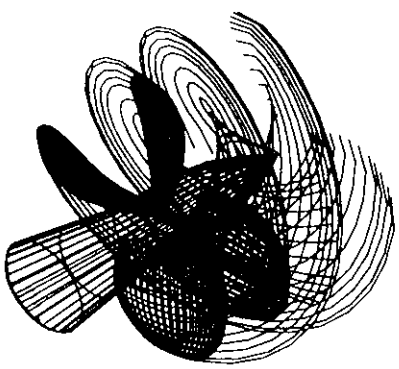

Fig. 2 Spiral trailing vortex lines behind a propeller in forward motion ($J = 0.6$).

Results of such a wake shedding procedure are shown in Fig. 2, after half a revolution of the propeller, which clearly indicates that the spiral shape of the trailing vortex lines is obtained directly from the kinematic motion of the propeller.

Solution of Eq. 15 will provide the velocity potential and the velocity components in the whole fluid region. Once the the flow field is determined the resulting pressures can be computed with the Bernoulli equation.

$$C_p = \frac{p - p_{ref}}{\frac{1}{2}\rho v_{ref}^2} = 1 - \frac{V^2}{v_{ref}^2} - \frac{2}{v_{ref}^2}\frac{\partial\Phi}{\partial t} \tag{17}$$

Here $\vec{V}$ and p are the local fluid velocity and pressure, p_{ref} is the far field reference pressure, and v_{ref} is the kinematic velocity as presented in Eq. 2.

$$\vec{v}_{ref} = -[\vec{V}_o + \vec{\Omega}\times\vec{r}] \tag{18}$$

A more useful form for the pressure coefficient for flows involving body rotation (see Ref. 13, p. 430) is:

$$C_p = \frac{p - p_{ref}}{\frac{1}{2}\rho v_{ref}^2} = -\frac{(\nabla\Phi)^2}{v_{ref}^2} + \frac{2}{v_{ref}^2}[\vec{V}_o + \vec{\Omega}\times\vec{r}]\cdot\nabla\Phi - \frac{2}{v_{ref}^2}\frac{\partial\Phi}{\partial t} \tag{19}$$

Note that in situations such as the forward motion of a propeller v_{ref} can be selected as the forward flight speed (V_o) or the local blade speed at each section on the propeller blade. The contribution of a panel with an area of ΔA_k to the aerodynamic loads $\Delta\vec{F}_k$ is thus

$$\Delta\vec{F}_k = -C_{p_k}(\frac{1}{2}\rho v_{ref}^2)_k \Delta A_k \vec{n}_k \tag{20}$$

(Note that v_{ref} here has a subscript k which means that it may change along the radius of the propeller blade.)

This panel model differs from the methods of Refs. 1-4 by its time dependent formulation. Furthermore, the ability to model relative motion between the various components of the body allows the treatment of flow fields such as that induced by a propeller in forward motion. This modified formulation has been incorporated into the latest version of the program PMARC[6].

Results

The capability to model propeller induced flow fields with the time dependent technique described above has been studied by comparing calculated data with experimentally derived values of pressure, thrust and torque. This comparison is based on the experimental results of Versmissen and van Gent[14] who tested a generic propeller/body at advance ratios of J=0.4 and 0.6. The panel representation of their experimental propeller/body is shown in Fig. 3. The propeller (in the experiment) had a diameter of 0.48 m and was tested in an open water tow-tank at forward speeds of 1.00 and 1.74m/sec (with corresponding rotational speeds of n=5.18 and n=6.02 revolutions per second). The geometrical model of the propeller/body consists of 2860 panels such that the central body consists of 660 panels and each of the propeller blades is represented by 550 panels. Fig. 4 depicts the front view of this four bladed propeller and the locations of the surface pressure measurement points on the suction side of one blade. Note that each propeller blade is twisted from root to tip by about 40 degrees. Test conditions and model geometry were aimed at obtaining attached flow conditions on the propeller with no visible cavitation.

The primary objective of such a numerical effort is to obtain a detailed surface pressure distribution on the propeller blades so that blade section shape can be optimized by the designer. This allows the tailoring of propeller blade loading in order to delay flow separations (by reducing leading edge suction peaks) or to reduce structural loads (by reducing blade-root bending moments), etc. The calculated pressure distributions for two different chordwise lines along

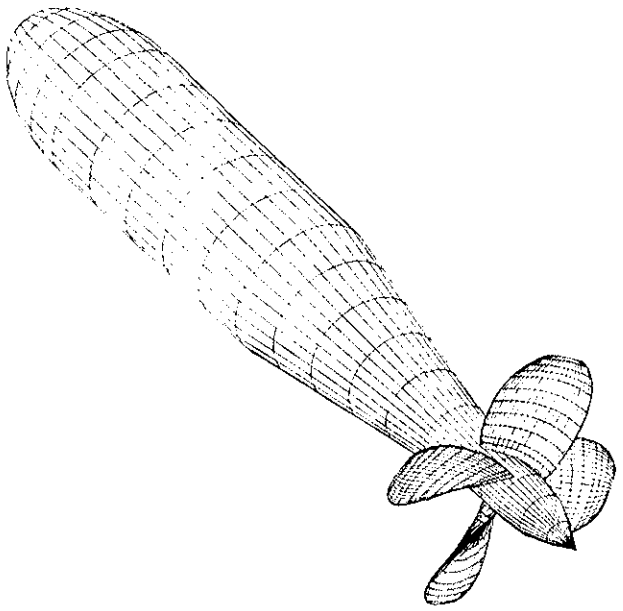

Fig. 3 Panel model for the propeller and the generic body (using 2860 panels).

the blade, for advance ratios of 0.4 and 0.6, are presented in Figs. 5 and 6. The corresponding shape of the propeller blade section is depicted in the inset to each of these figures. For a fixed blade pitch angle, the local airfoil section angle of attack increases as the advance ratio J is reduced. Therefore at J=0.4 the airfoil is producing more lift than at J=0.6, as shown by these figures. The experimental data for both the upper and lower surfaces compare reasonably well with the computational results. Experimentally derived pressures are not available near the leading and trailing edges due to experimental difficulties arising from the small blade thickness

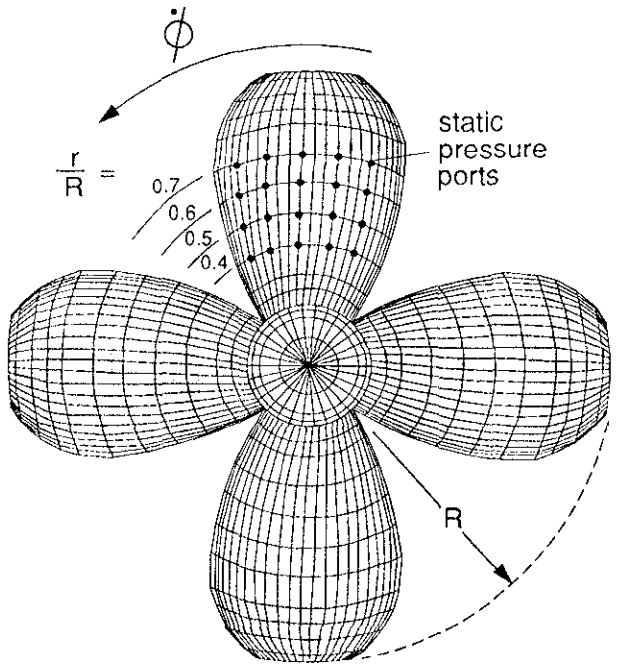

Fig. 4 Rear view of the four-bladed propeller and location of pressure ports in the experiments of Ref. 14.

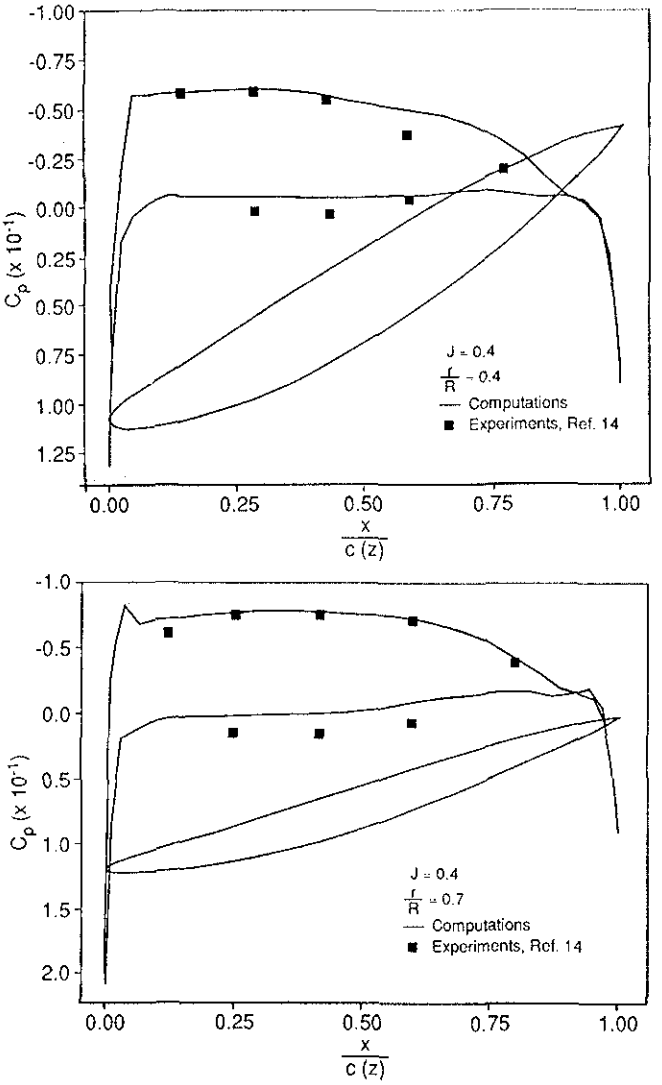

Fig. 5 Comparison between calculated and experimental pressure distribution on the propeller blade ($J = 0.4$, note that for this figure C_p is normalized by $v_{ref} = V_o$).

in these areas. Computations by Hess and Valarezo[8] using the same propeller geometry resulted in very similar pressure distributions, which can be viewed as a partial validation of the shape of the pressure distribution.

Propeller performance data can be calculated by integrating the surface pressures on all the panels and decomposing the result into thrust (axial) and torque (radial) components. With the present time stepping technique the propeller motion is initiated from rest so that the thrust and torque will stabilize only after the initial transient effects become negligible. For this particular geometry (shown in Fig. 3) the steady state condition was obtained after less than one revolution of the propeller*. In general, solutions obtained at higher advance ratios reach the steady state condition within fewer revolutions than those obtained at lower advance ratios. Bearing in mind that potential-flow based models are successful in predicting the lift of airfoils it is expected that the thrust coefficient calculated by this method will compare favorably with experimental data. Such data[14] were avail-

* This condition is usually obtained after 20 time steps, which required about 600 seconds on a CRAY-YMP computer.

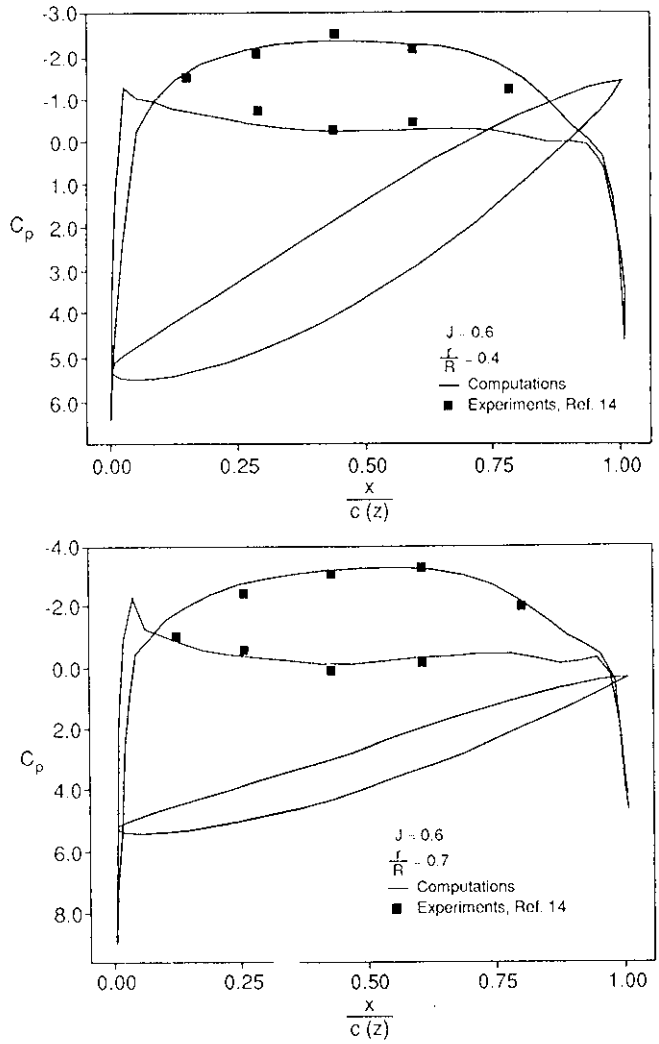

Fig. 6 Comparison between calculated and experimental pressure distribution on the propeller blade (J = 0.6, note that for this figure C_p is normalized by $v_{ref} = V_o$).

able only for β_{TIP} = 10°. The slope of the calculated curve $\Delta C_t/\Delta$ J in Fig. 7 (which is similar to the lift curve slope of an airfoil), is close to the slope of the experimental data, especially at the higher advance ratios. Viscous effects are expected to reduce the lift somewhat, so that the experimental results should be smaller than the calculated results. This is not the case in Fig. 7 and a possible explanation can be attributed to the small differences between the panel model and the actual propeller tested in Ref. 14 (e.g. a marginal discrepancy in blade pitch).

The torque coefficient data are presented in Fig. 8, and again the slope of the calculated curve is similar to the experimental result (available for β_{TIP} = 10° only and shown by the symbols in the figure). The larger torque values obtained experimentally are probably a result of the viscous effects which were not included in this model. For the lower advance ratios (larger blade angle of attack) these effects become larger and therefore the difference between the calculated and measured results increases. The effect of increasing blade pitch is to increase the blade loading and this is reflected in Figs. 7 and 8.

For completeness, calculated and measured propeller efficiency data are presented in Fig. 9. Since the efficiency is defined as $\eta = JC_T/2\pi C_Q$, it is clear that the viscous component of torque may have a dominant effect at certain advance ratios. At low advance ratios, thrust is high and torque is derived largely from surface pressure. Consequently, for J<0.5, the slope of the calculated efficiency curve is similar to the slope of the experimental data. For J>0.6, however, blade thrust becomes small whereas the viscous portion of the torque remains relatively large, resulting in the large loss in efficiency in this range. The computational results, which do not include a viscous component of torque, do not exhibit this effect.

Most panel methods are capable of computing the pressure distribution on complex bodies but from the propulsion integration point of view, estimation of propeller/body interaction becomes important. Earlier efforts to have a propeller grid rotating relative to a wing used low order panel methods[15] or even the laminar incompressible Navier-Stokes equations[16]. The capability to model similar flow conditions with the current unsteady method is demonstrated in Fig. 10 where the effect of the propeller on the pressure distribution along the body's centerline is depicted. The rectangular symbols show the calculated pressure coefficient for the axisymmetric body in the absence of a propeller. For the second computation (depicted by the solid circle symbols) the

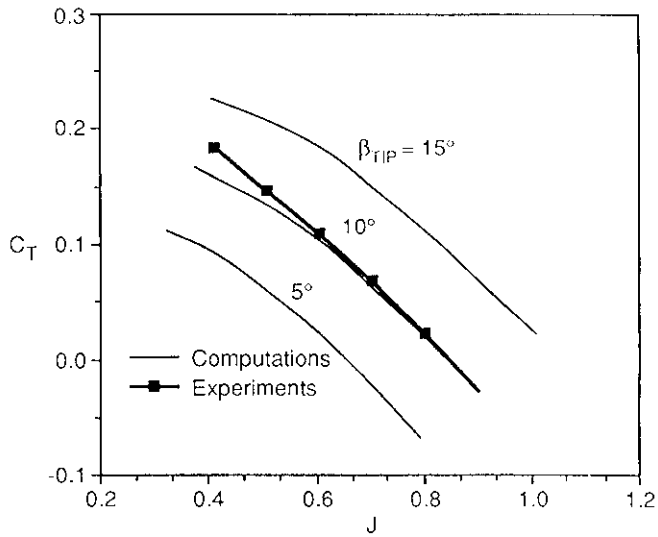

Fig. 7 Thrust coefficient versus advance ratio for the propeller of Fig. 4.

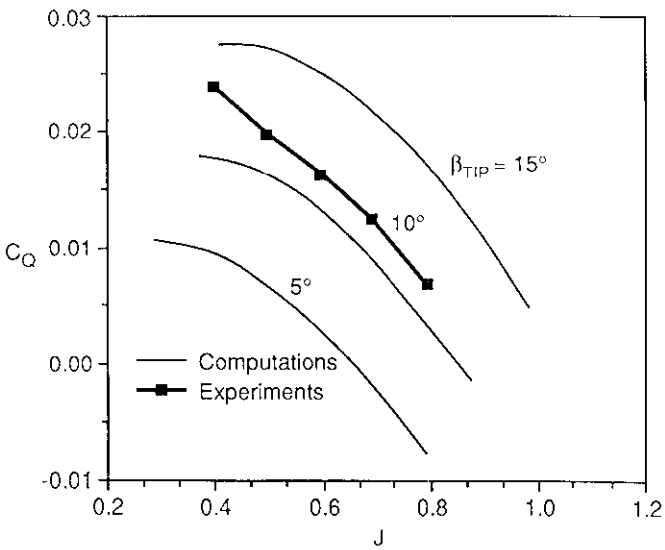

Fig. 8 Torque coefficient versus advance ratio for the propeller of Fig. 4.

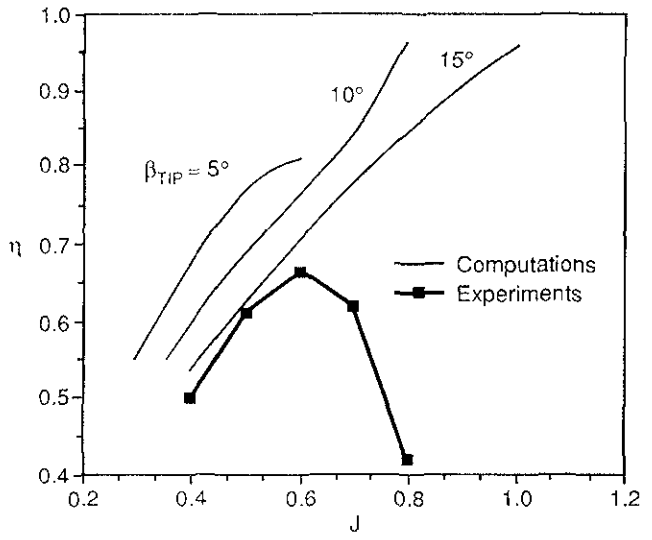

Fig. 9 Efficiency versus advance ratio for the propeller of Fig. 4.

propeller grid was added and rotated relative to the central body. The propeller seems to have a noticable effect on the body's aft section only, and clearly, it increases the pressure behind and reduces the pressure ahead of the blades. (One panel, though, was very near and influenced by the root wake line of the propeller and had a lower pressure coefficient, as shown by the arrow in Fig. 10.)

From a computational efficiency point of view, the body and propeller blades were initially modeled as shown in Fig. 3. A closer observation reveals that the propeller blades were lifted slightly above the central hub. The grid for this model is simpler to generate but the small gap between the hub and the blades causes a large pressure peak, which affects the pressure distribution on the axisymmetric body. Therefore, a modified panel model, shown in Fig. 11, was constructed in which the propeller and its hub were combined and rotated as a solid-body relative to the center-body and the rear end cone (which did not rotate). This modeling is posssible with the current panel code and the results of Fig. 10 were obtained by using this approach. Computational effort, though, increased slightly due to the relative motion between the body and propeller panels. This relative motion enforced a momentary update of some of the influence coefficients of Eq. 13 but such a model is more appropriate when the pressure distribution on the body is sought. The

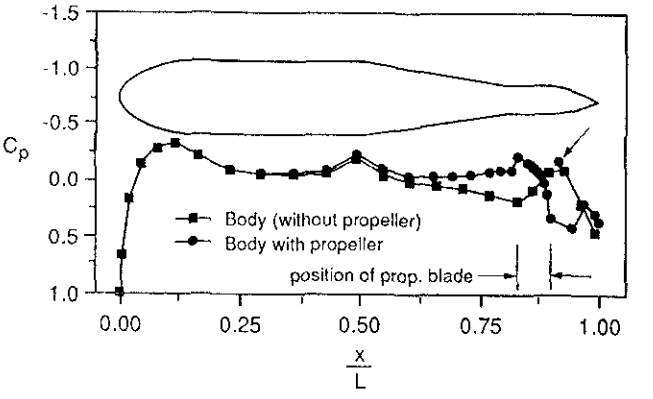

Fig. 10 Effect of propeller on the pressure distribution along the body's centerline.

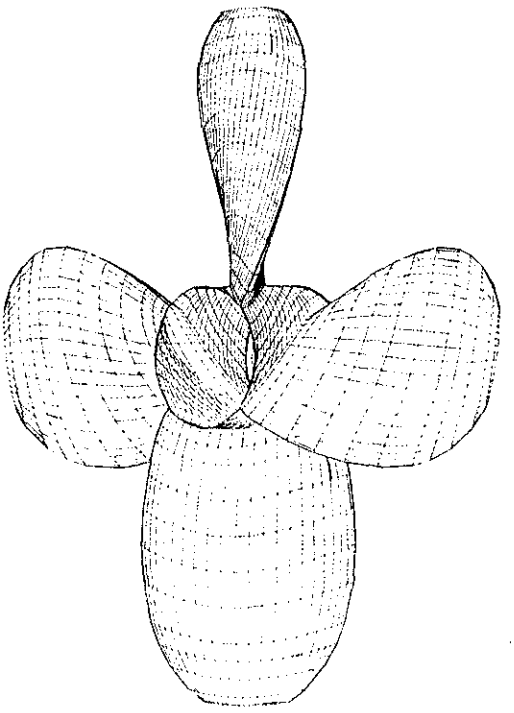

Fig. 11 Panel model for the rotating propeller/hub assembly.

pressure distribution on the propeller blades and the hydrodynamic coefficients (e.g. thrust and torque) are not affected by the difference between these two geometric panel models and therefore the computationally more economical configuration (of Fig. 3) was used to generate Figs. 7-9.

Conclusions

The present method is capable of modeling complex flow fields such as those created by a propeller rotating relative to a forward translating central body. Calculated pressure distributions on the propeller blade and the resulting pressure field on the body can be used for improving blade shape design and optimization of propeller performance, or can be used for structural design or noise reduction.

The method is limited only by the limits of the potential flow model which is applicable mainly to high-Reynolds number, incompressible, attached flows.

Acknowledgements

This work was supported by NASA Ames Research Center, under Grant No. NCC-2-458, with Dr. James C. Ross as project monitor.

References

1. Hess J., L. and Friedman, D. M.: An Improved High-Order Panel Method for Three-Dimensional Lifting Flow," Douglas Aircraft Co. Rep. No. NADC - 79277-60, 1981.

2. Maskew, B., "Program VSAERO, A Computer Program for Calculating the Nonlinear Aerodynamic Characteristics of Arbitrary Configurations," NASA CR-166476, Nov. 1982.

3. Youngren, H.H., Bouchard, E. E., Coopersmith, R. M., and Miranda L. R., "Comparison of Panel Method Formulations and its Influence on the Development of QUADPAN, an Advanced Low-Order Method," AIAA Paper 83-1827, 1983.

4. Magnus A. E. and Epton M. A. "PAN AIR - A Computer Program for Predicting Subsonic or Supersonic Linear Potential Flows About Arbitrary Configurations Using a Higher Order Panel Method, Volume 1 - Theory Document," NASA CR 3251, Nov 1983.

5. Katz, J. and Maskew B. "Unsteady Low-Speed Aerodynamic Model for Complete Aircraft Configurations," AIAA Paper 86-2180, Aug. 1986, Also, J. Aircraft Vol. 25, No. 4. 1988, pp. 302-310.

6. Ashby, L. D., Dudley, M. D., Iguchi, S. K., Browne, L., and Katz, J., Potential Flow Theory and Operation Guide for the Panel Code PMARC," NASA TM 102851, March 1990.

7. Kerwin, J. E., "Marine Propellers," Ann. Rev. Fluid Mech. Vol. 18, 1986, pp. 367-403.

8. Hess, J. L., and Valarezo, W. O., "Calculation of Steady Flow About Propellers Using a Surface Panel Method," J. Propulsion, Vol. 1, No. 6, 1985, pp. 470-476.

9. Valarezo, W. O., and Hess, J. L., "Time-Averaged Subsonic Propeller Flowfield Calculations," AIAA Paper No. 86-1807, June 1986.

10. Valarezo, W. O., and Liebeck, R. H., "Three Dimensional Calculation of Windmill Surface Pressures," AIAA Paper No. 88-2533, 1988.

11. Valarezo, W. O., "On the Use of Proplets as a Means for Reducing Blade Compressibility Losses," AIAA Paper No. 89-2213, August 1989.

12. Valarezo, W. O., "Calculation of Isolated and Installed Multiple Rotor Flows Using a Surface Panel Method," AIAA Paper No. 89-2214, August 1989.

13. Katz J. and Plotkin A., "Low-Speed Aerodynamics: From Wing Theory to Panel Methods," McGraw-Hill, Inc. New York, 1991.

14. Versmissen, G. G. P., and van Gent, W., "Hydrodynamic Pressure Measurements on a Ship Model Propeller," Proc. of the 14-th Symposium on Naval Hydrodynamics, National Academy Press, Washington D.C., 1983.

15. Rangwalla, A. A., and Wilson L. N., "Application of a Panel Code to Unsteady Wing-Propeller Interference," J. Aircraft, Vol. 24, No. 8, 1987, pp. 568-570.

16. Rajagopalan, R. G., and Moulton M. A., "A Numerical Study of a Wing and Propeller in Mutual Interference," AIAA Paper No. 89-2215, August 1989.